Surface characterizations of color thresholds

Allen B. Poirson, Brian A. Wandell, Denise C. Varner, and David H. Brainard

Department of Psychology, Stanford University, Stanford, California, 94305

Received August 8, 1988; revised manuscript received August 14, 1989; accepted December 11, 1989

We evaluate how well three different parametric shapes, ellipsoids, rectangles, and parallelograms, serve as models of three-dimensional detection contours. We describe how the procedures for deriving the best-fitting shapes constrain inferences about the theoretical visual detection mechanisms. The ellipsoidal shape, commonly assumed by vector-length theories, is related to a class of visual mechanisms that are unique only up to orthogonal transformations. The rectangle shape is related to a unique set of visual mechanisms, but since the rectangle is not invariant with respect to linear transformations the estimated visual mechanisms are dependent on the stimulus coordinate frame. The parallelogram is related to a unique set of visual mechanisms and can be derived by methods that are independent of the stimulus coordinate frame. We evaluate how well these shapes approximate detection contours, using 2-deg test fields with a long (1-sec) Gaussian time course. Two statistical tests suggest that the parallelogram model is too strong. First, we find that the ellipsoid and rectangle shapes fit the data with the same precision as the variance in repeated threshold measurements. The parallelogram model, which has more free parameters, fits the data with more precision than the variance in repeated threshold measurements. Second, although the parallelogram model provides a slightly better fit of our data than the other two shapes, it does not serve as a better guide than the ellipsoidal model for interpolating from the measurements to thresholds in novel color directions.

INTRODUCTION

Two approaches have dominated attempts to measure and understand visual sensitivity to small color differences. One approach, Stiles's two-color increment threshold measurements, was designed to explore the properties of visual mechanisms. In the increment threshold experiment the observer's state of adaptation is established by a large, steady background field; the observer's sensitivity is measured by sensitivity to a briefly presented test flash superimposed upon the background.[1,2] The observer's test or field sensitivity is summarized by spectral sensitivity curves made from measurements using monochromatic test and field lights.[3]

The second approach, MacAdam and Brown's measurements of color-matching variability,[4–6] was designed to characterize completely the visibility of small color differences. In the color-matching experiment the observer views a bipartite field with a test on one side and a mixture of color-matching primaries on the other side. The observer makes a series of color matches to the test. The observer's state of adaptation is established by the test; the observer's sensitivity is measured by the three-dimensional equal-variance contour calculated from the color matches. MacAdam and his colleagues noted that the matches are normally distributed, and thus the equal-variance contours are ellipsoidal. MacAdam and Brown assume that lights falling upon an ellipsoidal surface surrounding the test light's color coordinates are equally discriminable from the test light.[5,6]

MacAdam and Brown's use of a parametric surface to summarize discrimination contours is superior to summaries based on spectral sensitivity measurements. The choice of a parametric surface provides an interpolation rule that describes how to use a finite set of threshold measurements to predict sensitivity to all other colored lights. By comparison, no interpolation rule exists to use a finite set of spectral sensitivity measurements to predict sensitivity to other spectral lights or to mixtures of spectral lights.

A surface shape model of a detection contour is appropriate only if thresholds fall near the hypothesized surface. In this paper we perform a statistical analysis to evaluate the goodness of fit of the ellipsoidal, rectangular, and parallelogram shapes in characterizing thresholds measured with long-duration lights presented upon steady backgrounds.

METHODS

Experimental Procedure

The observer saw a background field that consisted either of a steadily presented 2-deg disk or a 2-deg disk surrounded by an annulus (4-deg outer diameter). The observer was asked to detect a 2-deg test field centered upon the background. The temporal modulation of the test was a truncated Gaussian ranging from −5 sd to +5 sd. These ten standard deviations took 1 sec. Each threshold was determined from at least 120 multiple-staircase, two-interval forced-choice trials. Weibull psychometric functions were fitted to the responses, using a maximum-likelihood method.[7] We report the 81% correct level as threshold.

Each detection contour was determined from thresholds measured in at least 15 vector directions in color space. Threshold detection contours were measured in 18 different adapting conditions, yielding 270 = 15 × 18 thresholds. Approximately 1800 = 15 × 120 forced-choice responses were used in determining the detection contours for a single adapting condition. Our results are derived from more than 32,000 forced-choice responses.

Threshold measurements were recorded at the instrument as the percent modulation of each monochromatic beam about the dc level. Using the known dc level and the stimulus percent modulation, we computed the difference in ener-

0740-3232/90/040783-07$02.00

gy between the peak of the Gaussian temporal modulation and the dc level of each monochromatic beam at threshold. We refer to the three-dimensional vector describing the colored test stimulus at threshold modulation as $\mathbf{t}$. The entries of the nth threshold measurement, $\mathbf{t}_n$, are the contrast modulations of the three primary lights, $\mathbf{t}_n = (t_{n1}, t_{n2}, t_{n3})$.

Threshold Symmetries

All the parametric shapes that we evaluate here, ellipsoid, rectangle, and parallelogram, are symmetric around the origin. This implies that increments and decrements along the same vector direction should have the same threshold visibility. In preparation for this work, we made measurements quite similar to those reported here. We found that, under our viewing conditions, observers are equally sensitive to increments and decrements in the same vector direction of color space. For this study we did not attempt to replicate this observation. Rather, we measured thresholds on one side of a plane dividing color space and assumed that increment and decrement thresholds are identical.

Stromeyer *et al.* (Ref. 8, Figs. 4 and 5 and Table 1) and Kranda and King-Smith (Ref. 9, Fig. 6b) report asymmetries that are inconsistent with the ellipsoidal approximation. Stromeyer *et al.* report that "... the asymmetries observed with chromatic flashes virtually disappeared when the duration of the flash was simply increased to 200 msec" (p. 226). Our test measurements were all restricted to the conditions in which we and Stromeyer *et al.* found symmetric detection contours.

Apparatus

Our measurements were made using a four-channel Maxwellian view. The first three channels contained closed-loop feedback control and are described in an earlier publication.[10] The lights from three of the four channels served as the test stimulus primaries. We used narrow-band interference filters, placed before the feedback measurements, to render each of the test stimulus primaries monochromatic. The interference filter wavelengths were 480, 650, and 540 nm. For the present experiments we added one more channel, optically identical to the first three but without the closed-loop feedback. The fourth channel provided the adapting field. The spectral distribution of the fourth channel was controlled by interference filters or broadband colored filters, depending on the condition.

Calibration

We measured light levels with a silicon photodiode (United Detector Technologies PIN-10). At the beginning of each day we adjusted the dc level of each monochromatic beam, using neutral-density wedges placed in each beam path. From the photodiode measurements we computed the dc level in units of log quanta sec^{-1} deg^{-2}. We report these values in the figure captions. Only small adjustments in the neutral-density filters were necessary to maintain constant levels since day-to-day variability of beam intensity was typically 1% or less.

Observers

Three observers took part in our experiments. Two observers (PC and DR) had normal color vision determined by the H-R-R pseudoisochromatic plate test and by anomaloscopy. One observer (observer DV) had a mild deutan defect. This observer's Rayleigh matches are on the color-normal extreme of the deutan distribution (26–30 Nagel units); the observer failed two plates of H-R-R and passed the 15-hue test.

Fitting Surfaces to the Threshold Data

General Framework

The procedures for fitting the three surface shapes, ellipsoids, rectangles, and parallelograms, to threshold data can be described by using a common framework. We first map the threshold data into a new coordinate frame, using a linear transformation, $\mathbf{m}_n = \mathbf{A}\mathbf{t}_n$. We call the new coordinate frame the privileged coordinate frame. The quantity $(\sum_{j=1,3} m_{nj}{}^{\gamma})^{1/\gamma}$ is the Minkowski length of the vector, $\mathbf{m}_n$. Were there no measurement error, we would expect thresholds represented in the privileged coordinate frame to fall upon a surface of, say, unit Minkowski length,

$$\left(\sum_{j=1,3} m_{nj}{}^{\gamma}\right)^{1/\gamma} = 1.0. \tag{1}$$

As we describe in detail below, differences between the three surface shapes we use to describe threshold can be stated in terms of the restrictions on the transformation into the privileged coordinate frame, $\mathbf{A}$, and the value of the exponent γ used to define the Minkowski length. When we fit different surface shape models, we search for a linear transformation, $\mathbf{A}$, that minimizes the sum of squared errors between the Minkowski length of the transformed data and 1.0, that is,

$$\sum_n \left[\left(\sum_{j=1,3} m_{nj}{}^{\gamma}\right)^{1/\gamma} - 1.0\right]^2. \tag{2}$$

In our fitting procedures we make extensive use of the fact that any linear transformation $\mathbf{A}$ can be decomposed by the singular value decomposition into $\mathbf{A} = \mathbf{U}\mathbf{S}\mathbf{V}^t$. The matrices $\mathbf{U}$ and $\mathbf{V}$ are orthogonal, and the matrix $\mathbf{S}$ is diagonal with all positive entries. Once we have determined the restrictions on $\mathbf{A}$ and γ imposed by a surface model, we search for the best solution, using STEPIT, Chandler's[11] iterative search program.

Ellipsoids

Threshold data will be fitted by an ellipsoid centered on the origin if the linear transformation $\mathbf{A}$ maps the thresholds into a unit sphere in the privileged coordinate frame. Points on the unit sphere have an equal Minkowski length when $\gamma = 2.0$. In this case Eq. (1) reduces to the usual equation for vector length. We can use compact matrix notation to express Eq. (1) as $(\mathbf{m}_n{}^t\mathbf{m}_n)^{1/2} = (\mathbf{t}_n{}^t\mathbf{A}^t\mathbf{A}\mathbf{t}_n)^{1/2} = 1.0$. Notice that $\mathbf{A}^t\mathbf{A} = \mathbf{Q}$ is a symmetric, positive-definite matrix and that

$$\mathbf{t}_n{}^t\mathbf{Q}\mathbf{t}_n = 1.0 \tag{3}$$

is the matrix form for describing an ellipsoid. Some prefer the expansive summation notation for this equation,

$$\begin{aligned} &Q_{11}t_{n1}{}^2 + 2Q_{12}t_{n1}t_{n2} + 2Q_{13}t_{n1}t_{n3} \\ &\quad + Q_{22}t_{n2}{}^2 + 2Q_{23}t_{n2}t_{n3} \\ &\quad + Q_{33}t_{n3}{}^2 = 1.0, \end{aligned} \tag{4}$$

where the ijth entry of $\mathbf{Q}$ is $Q_{ij} = Q_{ji}$.

From Eq. (3) or (4) we see that the ellipsoidal approximation to the data depends not explicitly on the matrix $\mathbf{A}$ but only on the matrix $\mathbf{Q} = \mathbf{A}^t\mathbf{A}$. Since $\mathbf{A}^t\mathbf{A} = \mathbf{V}\mathbf{S}^2\mathbf{V}^t$, the quality of the approximation is independent of the orthogonal transformation $\mathbf{U}$. Any choice of an orthogonal matrix $\mathbf{U}$ yields a matrix, $\mathbf{A} = \mathbf{U}\mathbf{S}\mathbf{V}^t$, that serves equally well as a candidate transformation from the stimulus cooordinate frame to the privileged coordinate frame. It follows that we cannot use the ellipsoidal surface model to estimate a unique transformation from stimulus coordinates to the privileged coordinate frame by using only one threshold data set.

To estimate the best ellipsoidal fit, we set $\mathbf{U}$ to the identity and have STEPIT search for a matrix $\mathbf{A} = \mathbf{S}\mathbf{V}^t$ that minimizes the sum of squared errors in expression (2) with $\gamma = 2.0$. Six parameters are required in order to define $\mathbf{A}$ in the ellipsoid model, three to specify the orthogonal transformation $\mathbf{V}$, and three to specify the diagonal entries in $\mathbf{S}$.

Rectangles and Parallelograms

Rectangular and parallelogram models of the detection contour both correspond to fitting the data with unit cubes in the privileged coordinate frame. Points on the unit cube have equal Minkowski length when $\gamma = \infty$. In this case Eq. (1) reduces to

$$\mathrm{MAX}_j(m_{nj}) = 1.0. \tag{5}$$

The rectangular and parallelogram fits differ in their restrictions on the linear transformation $\mathbf{A}$. If we restrict $\mathbf{U} = \mathbf{I}$ so that $\mathbf{A} = \mathbf{S}\mathbf{V}^t$, then we will fit a rectangle in stimulus coordinates to the data points. If we do not restrict $\mathbf{U}$, so that the mapping from stimulus coordinates to the privileged coordinate frame is a general matrix, $\mathbf{A} = \mathbf{U}\mathbf{S}\mathbf{V}^t$, then we will fit a parallelogram to the data points. Six parameters are required to define $\mathbf{A}$ in the rectangle model, and nine parameters are required to define $\mathbf{A}$ in the parallelogram model. The rectangle model is a special case of the parallelogram model.

Coordinate Frame Independence

For the ellipsoidal and parallelogram shapes the error function used to guide the STEPIT minimization [expression (2)] returns an estimate of the privileged coordinate frame that is independent of the stimulus coordinate frame. Compare the solutions when the data are represented in two coordinate frames related by the linear transformation $\mathbf{t}_n' = \mathbf{L}\mathbf{t}_n$. When we start with the data represented as $\mathbf{t}_n$, we will find the transformation $\hat{\mathbf{A}}_1\mathbf{t}_n$ that yields the smallest error. Suppose that the transformation from $\mathbf{t}_n'$ to the privileged coordinate frame does not differ by $\mathbf{L}$, that is, suppose that $\hat{\mathbf{A}}_2 \neq \hat{\mathbf{A}}_1\mathbf{L}^{-1}$. Then the error estimated using $\hat{\mathbf{A}}_2\mathbf{t}_n'$ is less than all other linear transformations; in particular, it is less than the error estimated using $\hat{\mathbf{A}}_1\mathbf{L}^{-1}\mathbf{t}_n' = \hat{\mathbf{A}}_1\mathbf{t}_n$. But we have already asserted that the error obtained by $\hat{\mathbf{A}}_1\mathbf{t}_n$ is the smallest error. So it must be that $\hat{\mathbf{A}}_2 = \hat{\mathbf{A}}_1\mathbf{L}^{-1}$.

The error evaluation equation for the rectangle shape is not independent across all linear transformations of the stimulus coordinate frame. The difference between the rectangle shape and the ellipsoid and parallelogram shapes is that that rectangle shape is not invariant with respect to linear transformations. Under a linear transformation the rectangle can become a parallelogram. Put in terms of restrictions on $\mathbf{A}$, when the rectangle is fitted in the first stimulus coordinate frame the matrix $\hat{\mathbf{A}}_1$ is restricted to be of the form $\hat{\mathbf{A}}_1 = \mathbf{S}_1\mathbf{V}_1^t$. The matrix yielding the same error in the second stimulus coordinate frame, $\hat{\mathbf{A}}_2 = \hat{\mathbf{A}}_1\mathbf{L}^{-1}$, may not be of the general form $\mathbf{S}_2\mathbf{V}_2^t$. When we report the error for the rectangular approximation to our data, our calculations are made with respect to the stimulus coordinate frame of our data described above. We view the coordinate frame dependence of the rectangle as a severe shortcoming of this surface model.

Viewing the Three-Dimensional Surfaces

In Fig. 1 we plot graphs that show the data and cross sections of fitted surfaces in three planes. In each of the diagrams the solid line describes a slice through the parallelogram, the dashed line is a slice through the rectangle, and the dotted line is a slice through the ellipsoid. The three planes were selected by choosing two of the three stimulus primaries as axes. The plotted points are contrast detection thresholds for stimuli within the plane. Additional measurements made with mixtures of all three primaries were also used to fit the surfaces; since these measurements are not in any of the three planes plotted, they cannot be shown in this type of figure.

In color directions for which we have measured thresholds, the predictions of the three different shapes are quite similar. Where there are no measurements, the shapes differ in their threshold predictions. For example, consider the top diagram in Fig. 1. If we use the best-fitting parallelogram to interpolate between threshold measurements, then the predicted threshold in the 45-deg direction is roughly twice as large as that of the ellipsoidal or rectangular predictions.

Visual Mechanisms

The assumption that an ellipsoidal surface can be used to describe the detection contour plays an important role in vector-length theories. Theorists working with vector-length theories[12–15] treat the axes of the privileged coordinate frame as defining fundamental visual mechanisms of color vision and interpret these coordinates in terms of physiological mechanisms. Since the ellipsoidal model does not permit us to recover $\mathbf{A}$ uniquely, it does not permit us to identify the fundamental visual mechanisms in a vector-length model from a single detection contour.

Unlike in the ellipsoidal case, it is possible to use either rectangular or parallelogram fits to the data to specify uniquely the mapping $\mathbf{A}$, up to reordering the rows of the matrix. For the rectangle shape, however, the inferred privileged coordinate frame depends on the choice of stimulus coordinate frame. Only the parallelogram model yields a unique privileged coordinate that is independent of the stimulus coordinate frame.

RESULTS

Quality of the Surface Approximations

We have compared three fits to our data, using the ellipsoid, rectangle, and parallelogram shapes. As we described in the Methods section, fits to the data made using the ellipsoid and rectangle shapes require six parameters, while the parallelogram shape requires nine parameters.

For each of the three surface shapes, we searched for a linear transformation into the privileged coordinate frame such that the Minkowski length of the transformed data is 1.

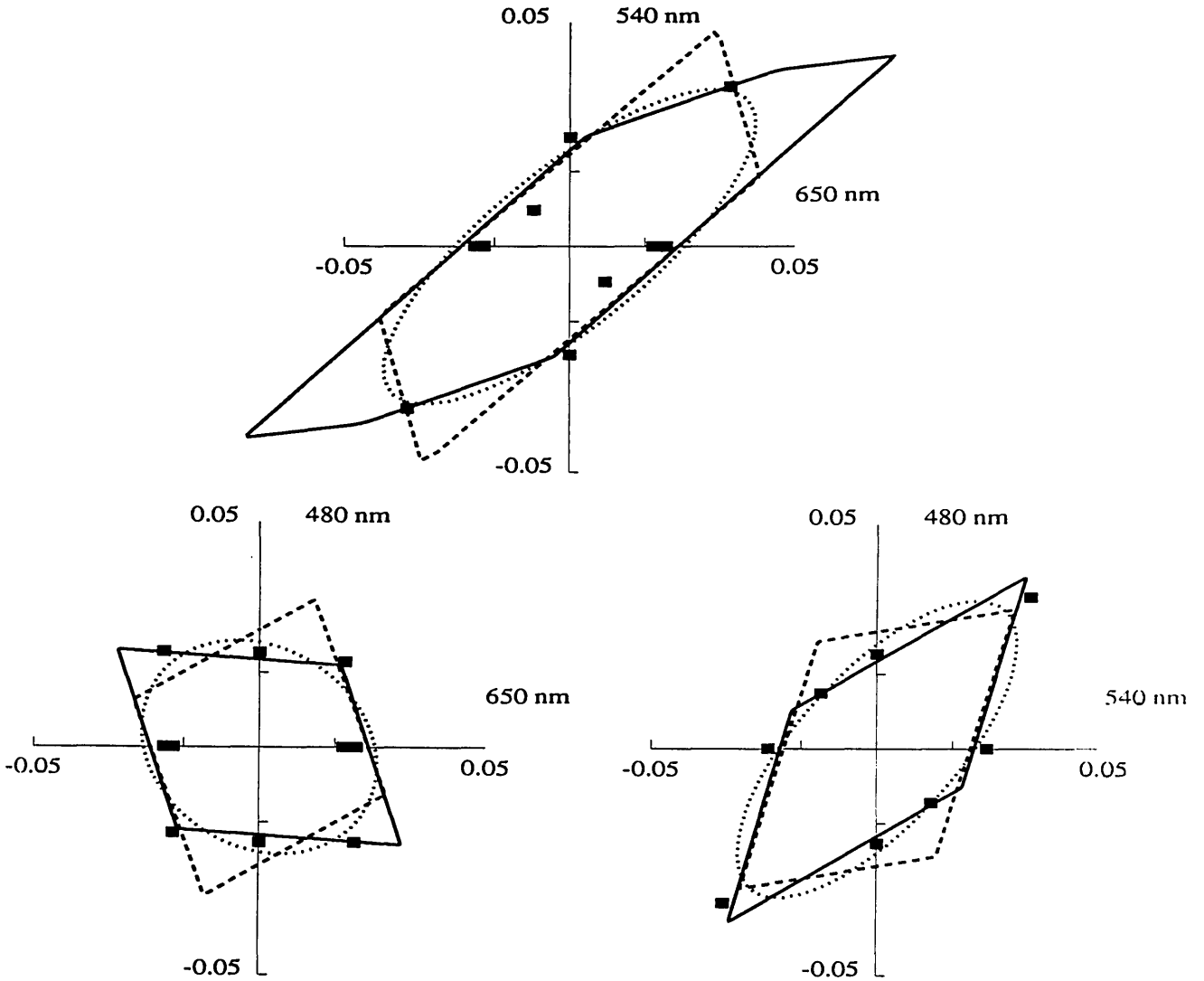

Fig. 1. Thresholds (filled symbols) and cross sections of fitted surfaces (curves) in three color planes. The axes are the percent contrast modulation at detection threshold for the test stimulus primaries. Thresholds were measured on a white, 2-deg background field, surrounded by a 490-nm annulus with an outer diameter of 4 deg. The white disk was formed by the mixture of 480-, 650-, and 540-nm lights at 9.250, 9.609, and 9.103 log quanta sec^{-1} deg^{-2}, respectively. The annulus intensity was 9.708 log quanta sec^{-1} deg^{-2}. The cross sections are from parallelogram (solid lines), rectangle (dashed lines), and ellipsoid (dotted curves) shapes.

For each of the shapes, we plot in Fig. 2 binned frequencies of the Minkowski lengths of the data in the privileged coordinate frame. A shape fits the data perfectly if the frequency distribution of Minkowski lengths is a spike at 1.0.

There is no significant difference between the frequency distributions for the ellipsoidal and rectangular fits. In both cases 70% of the data have a Minkowski length differing from 1.0 by less than 0.10 log unit, and 85% of the data have a Minkowski length differing by less than 0.15 log unit, from 1.0. The parallelogram fit requires three additional parameters and contains the rectangular fit as a special case. The parallelogram model provides the best approximation; 80% of the thresholds have a Minkowski length differing from 1.0 by less than 0.10 log unit, and 90% of the thresholds have a Minkowski length differing by less than 0.15 log unit from 1.0. The parallelogram model improves the fit, but the model uses nine parameters to fit the data.

Replications of Threshold Measurements

We can compare the deviations from unit length with what we would expect to find if we simply repeat the threshold measurements. Observer DV replicated threshold measurements in four color directions. For each of the four color directions, DV ran 5 replications of 120 trials. We use the pooled data in each color direction, all $5 \times 120 = 600$ observations as the true estimate of threshold in that direction. We call the ratio of the individual replications to the pooled threshold estimate the normalized threshold. Because the ratios are derived from thresholds that fall upon a common line in color space, the value is invariant under all linear transformations. Were there no variability across replications, the normalized threshold values would all be 1.0.

Twenty replications are sufficient to define a frequency distribution that is stable near the center but not at the

extreme values. In Fig. 3 we plot the cumulative distribution of the normalized thresholds (open circles) along with the cumulative distribution of the Minkowski lengths for the ellipsoidal (crosses), rectangular (filled squares), and parallelogram (filled diamonds) fits to the data. The cumulative frequency distributions of the Minkowski lengths for the different shapes are computed from the distributions in Fig. 2. In the central part of the curve, where our estimates are most stable, the ellipsoidal and rectangular model errors fall precisely upon the cumulative frequency distribution of the normalized thresholds. The parallelogram fit has less variance than the data replications (the curve is steeper). To reject the ellipsoidal model in favor of the parallelogram model would require us to reduce the measurement error. Based on the number and distribution of our measurements, we cannot be confident that the parallelogram model provides a better fit to the data.

Further Comparison of the Models

We have performed a second statistical analysis that compares how well the parallelogram and ellipsoidal shapes guide us in interpolating from the measurements to predict thresholds in other color directions. We randomly selected 13 measurements from the data set illustrated in Fig. 1. The complete data set consists of 16 threshold measurements. For 100 random selections of 13 points, we estimated the best-fitting parallelogram and ellipsoid. As for the data set as a whole, we find that the standard deviation of the difference between the predicted and observed thresholds for the parallelogram shape is slightly smaller (0.146) than the difference between the predicted and observed thresholds for the ellipsoidal shape (0.154).

The standard deviation between the predicted and observed thresholds for the three points excluded from each of the fits, however, is larger when we interpolate based on the parallelogram shape (0.393) than when we interpolate based on the ellipsoidal shape (0.303). We conclude that predictions interpolated from the parallelogram shape are no better than predictions interpolated from the ellipsoidal shape.

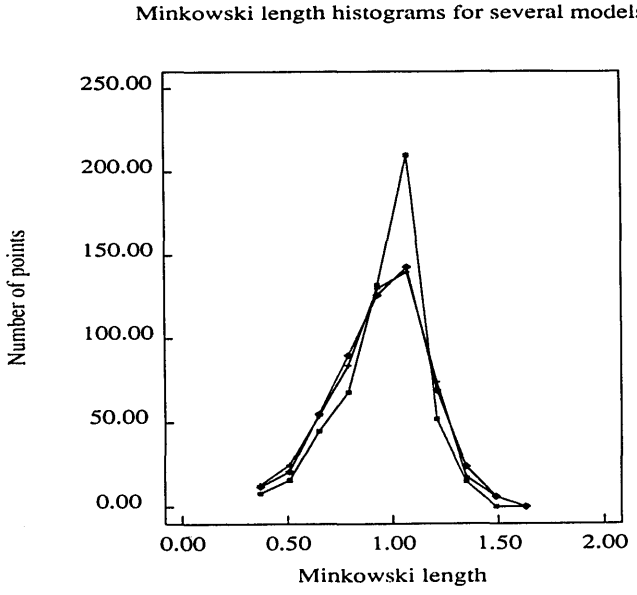

Fig. 2. Minkowski length frequency distributions for the three different shapes: ellipsoidal (crosses), rectangular (filled diamonds), and parallelogram (filled boxes). If any of the shapes fitted perfectly, then the corresponding Minkowski length distribution would be a delta function at 1.

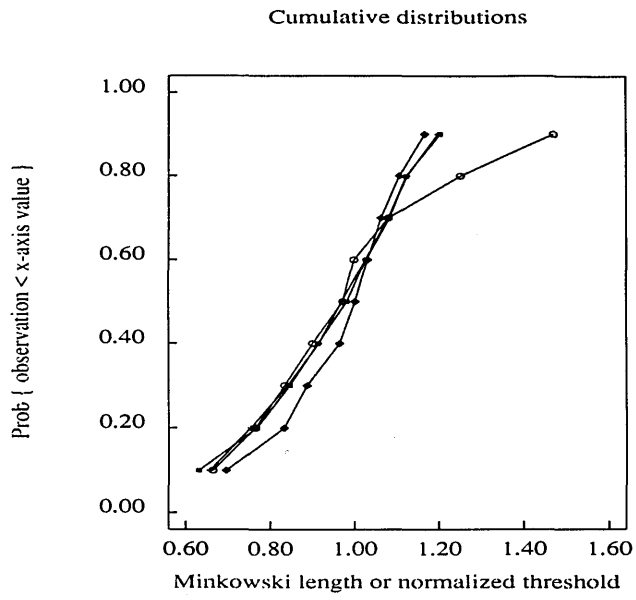

Fig. 3. Cumulative frequency distribution of the normalized thresholds (open circles) and cumulative distributions of the Minkowski lengths of the ellipsoidal (crosses), rectangular (filled squares) and parallelogram (filled diamonds) shapes.

Spectral Sensitivity Estimates

Once we accept a surface shape as a model of the detection contour, then we can estimate sensitivity to test lights in any direction in color space. To estimate threshold to an arbitrary test light, however, requires us to specify the vector of our stimulus primaries that are a metameric match to the arbitrary test light. Without measuring this color match directly, we cannot be certain what the metameric match would be. But we can use the color-matching functions of the standard observer to predict approximately what the match would be.

As an example, we calculate predicted observer spectral sensitivities from the ellipsoidal fit to detection data. First, we estimate the quadratic $\mathbf{Q}$. Then, assuming that observer PC's color-matching functions are equal to the Judd[16] modification of the CIE 1931 color-matching functions, we can find a vector direction, $\mathbf{p}$, that is a color match to any arbitrary test light. Finally, we can find the predicted threshold intensity of $\mathbf{p}$ by solving for the scalar constant α_p such that $(\alpha_p\mathbf{p})^t\mathbf{Q}(\alpha_p\mathbf{p}) = 1.0$

In Fig. 4 we plot the log spectral sensitivity $[-\log(\alpha_p)]$ derived from the estimated ellipsoid in one adapting condition for observer PC. The log spectral sensitivity curve derived from the ellipsoid is compared with two spectral sensitivity curves obtained by direct measurement, reported by Sperling and Harwerth.[17] For observer PC the background field was achromatic in appearance and 2 deg in diameter (see the caption to Fig. 4 for more details). The test field was also 2 deg and was superimposed upon the background. Sperling and Harwerth measured sensitivity using a briefly flashed, 45-min foveal test field superimposed upon a 10-deg background field. The correspondence between the directly measured spectral sensitivity curves and

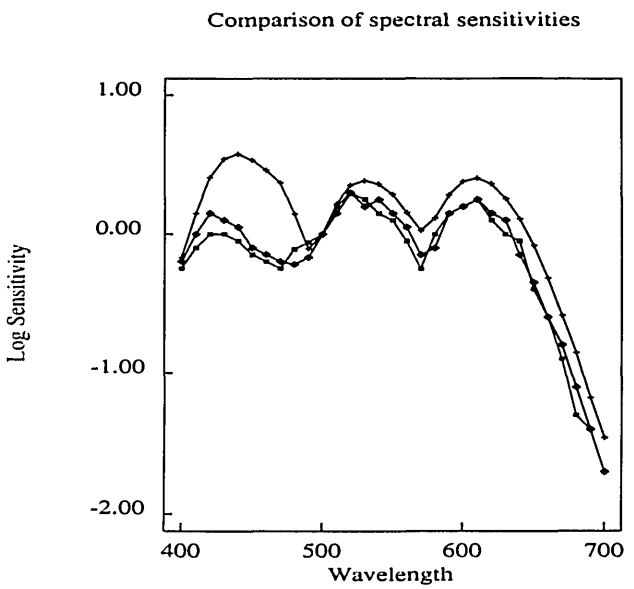

Fig. 4. Spectral sensitivities derived from observer PC's ellipsoids (crosses) compared with spectral sensitivity measurements from two observers (filled symbols) measured on 4-log Td, 10-deg achromatic backgrounds, as described by Sperling and Harwerth.[17] Observer PC viewed a 2-deg achromatic background field formed by the mixture of 480-, 650-, and 540-nm lights at 8.755, 9.544, and 9.000 log quanta sec^{-1} deg^{-2}, respectively. The test field was also 2 deg, centered upon the background. To facilitate comparison of the curves, the data have been shifted to coincide at 500 nm. Since the test field seen by PC is larger, longer in duration, and more gradual in its onset and offset than the one used by Sperling and Harwerth, we expect his sensitivity to be relatively greater in the short-wavelength region.

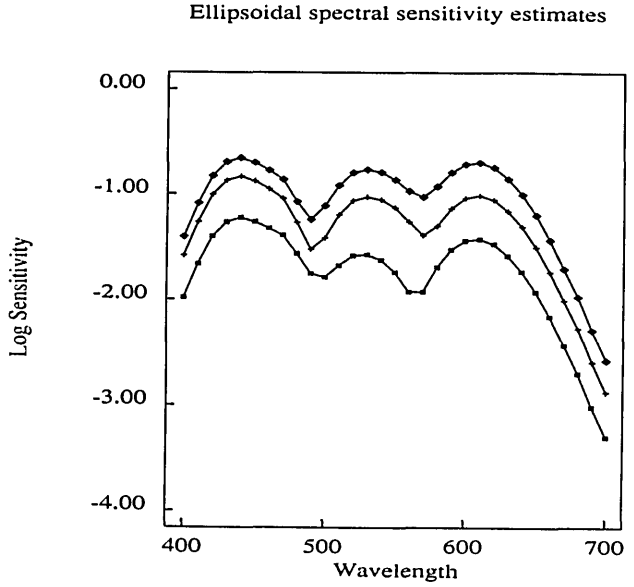

Fig. 5. Observer PC's spectral sensitivity curves derived from the ellipsoidal approximation to data collected at three intensities of the achromatic background field. If we call the intensity of the achromatic test field 1.0 in the first condition, then the intensities in the second and third conditions are 2.0 and 6.0, respectively. The spectral sensitivity curve derived in condition one is the top curve (filled diamonds), in condition two is the middle curve (crosses), and in condition three is the bottom curve (filled squares). The log quanta sec^{-1} deg^{-2} values for the 480-, 650- and 540-nm components were, respectively, 8.434, 9.243, and 8.699 for condition one, 8.755, 9.544, and 9.000 for condition two, and 9.232, 10.021, and 9.477 for condition three.

the indirectly inferred spectral sensitivity curves is quite good. The increased sensitivity of observer PC in the short-wavelength region is almost certainly due to the larger size and longer duration of the test stimulus used in the present study.

Figure 5 compares the derived spectral sensitivity curves for observer PC as the intensity of the achromatic background is increased over a factor of 6.0. The curves shift down as the intensity of the achromatic background field increases. The characteristic lobes remain present, although their peak wavelength can be seen to change slightly as the intensity of the achromatic background field increases. These data are consistent with the data reported by Sperling and Harwerth.

CONCLUSION

The best-fitting ellipsoid approximates our threshold data with the same precision as replications of the data. The ellipsoidal fit to the data is obtained by using methods that are independent of the stimulus coordinate frame. Even though the ellipsoidal fit is unique, no single set of visual mechanisms can be derived from one ellipsoidal shape. Estimates of the visual mechanisms derived from the ellipsoidal approximation to the data are unique only up to an orthogonal transformation.

The rectangle shape is geometrically similar to the ellipsoid, so it is not surprising that the rectangle approximates the data equally well. While the relationship between the rectangular shape and visual mechanisms is unique, the derivation of the visual mechanisms is dependent on the coordinate frame chosen for the stimulus representation. The rectangle shape, therefore, is satisfactory as an empirical approximation of the data but is unsatisfactory as a theoretical means of identifying visual mechanisms.

The parallelogram shape generalizes the rectangle shape and eliminates the dependence between inferred visual mechanisms and the stimulus coordinate frame. From the parallelogram fit we can identify a unique set of visual mechanisms based on methods that are independent of the stimulus coordinate frame. The parallelogram model fits many of our data sets slightly better than the ellipsoidal model, probably because it has more free parameters. But the parallelogram model does not serve as a better guide for interpolating beyond the data than the ellipsoidal model.

ACKNOWLEDGMENTS

This research was supported by National Eye Institute grant 2 RO1 EY03164 and NASA grants NCC 2-307 and NCC 2-332. We thank A. Ahumada and V. Pratt for useful discussions.

REFERENCES

1. W. S. Stiles, "The directional sensitivity of the retina and the spectral sensitivities of the rods and cones," Proc. R. Soc. London Ser. B 127, 64–105 (1939).
2. W. S. Stiles, "Color vision: the approach through increment-threshold sensitivity," Proc. Natl. Acad. Sci. USA 45, 100–114 (1959).

3. W. S. Stiles, in *Mechanisms of Colour Vision*, (Academic, London, 1978).
4. D. L. MacAdam, "Visual sensitivities to color differences in daylight," J. Opt. Soc. Am. **32,** 247–274 (1942).
5. W. R. J. Brown and D. L. MacAdam, "Visual sensitivities to combined chromaticity and luminance differences," J. Opt. Soc. Am. **39,** 808–834 (1949).
6. W. R. J. Brown, "Color discrimination of twelve observers," J. Opt. Soc. Am. **47,** 137–143 (1957).
7. A. B. Watson, "Probability summation over time," Vision Res. **19,** 515–522 (1979).
8. C. F. Stromeyer III, G. R. Cole, and R. E. Kronauer, "Second-site adaptation in the red-green chromatic pathways," Vision Res. **25,** 219–237 (1985).
9. K. Kranda and P. E. King-Smith, "Detection of coloured stimuli by independent linear systems," Vision Res. **19,** 733–746 (1979).
10. B. A. Wandell, "Color measurement and discrimination," J. Opt. Soc. Am. A **2,** 62–71 (1985).
11. J. P. Chandler, STEPIT, Quantum Chemistry Program Exchange, Department of Chemistry, Indiana University, Bloomington, Ind. (1965).
12. S. L. Guth, "Non-additivity and inhibition among chromatic luminances at threshold," Vision Res. **7,** 319–328 (1967).
13. S. L. Guth and H. R. Lodge, "Heterochromatic additivity, foveal spectral sensitivity, and a new color model," J. Opt. Soc. Am. **63,** 450–462 (1973).
14. S. L. Guth, R. W. Massof, and T. Benzschawel, "Vector model for normal and dichromatic color vision," J. Opt. Soc. Am. **70,** 197–212 (1980).
15. C. R. Ingling and B. H-P Tsou, "Orthogonal combination of the three visual channels," Vision Res. **17,** 1075–1082 (1977).
16. D. B. Judd; "Report of the U.S. Secretariat Committee on Colorimetry and Artificial Daylight," in *CIE Proceedings* (Bureau de la CIE, Paris, 1951), Vol. 1, Part 7, p. 11.
17. H. G. Sperling and R. S. Harwerth, "Red-green cone interactions in the increment-threshold spectral sensitivity of primates," Science **172,** 180–184 (1971).